



TECHNICAL PAPER

Static behavior of RC deck slabs partially prestressed with hybrid fiber reinforced polymer tendons

Xin Wang¹ | Nageh M. Ali¹ | Lining Ding² | Jianzhe Shi¹ | Zhishen Wu¹

¹Key Laboratory of C & PC Structures Ministry of Education, Southeast University, Nanjing, China

²School of Civil Engineering, Nanjing Forestry University, Nanjing, China

Correspondence

Zhishen Wu, Key Laboratory of C & PC Structures Ministry of Education, Southeast University, Nanjing 210096, China
Email: zswu@seu.edu.cn

Funding information

National Key Research and Development Program of China, Grant/Award Number: 2017YFC0703000; Natural Science Foundation of Jiangsu Province, Grant/Award Number: BK20150886; National Natural Science Foundation of China, Grant/Award Number: NSFC 51508277 and NSFC 51678139

The design of traditional FRP-RC deck slabs incurs a waste of FRP due to the minimum limit of reinforcement ratio recommended by the current design specifications. This paper investigates the static behaviors of full-scale RC deck slabs transversely reinforced and prestressed with basalt/carbon fiber reinforced polymer (FRP) hybrid tendons, which are capable of enhancing the utilization efficiency of FRP reinforcement. Two nonprestressed control deck slabs and five prestressed FRP-RC deck slabs were tested up to failure. The experimental variables included FRP-reduction factor, prestress level and partial prestressing index. The results indicate that the amount of bottom transverse reinforcement of FRP-RC deck slabs is reduced by 45% through introducing prestressing into FRP reinforcement. Those three variables have negligible effect on the failure mode of the prestressed FRP-RC deck slabs. The FRP-reduction factor primarily affects the ultimate load and cracking load, crack width, and strain in nonprestressing reinforcements and concrete. Prestressing level has significant effects on the cracking load, deflection, crack width and strain in nonprestressed reinforcements. By contrast, partial prestressing index has no effect on the static behaviors of the FRP-RC deck slabs. Furthermore, the residual crack width and deflection of FRP-RC deck slabs are controlled significantly by prestressing, which contributes to realizing a superior long-term behavior of the deck slabs.

KEY WORDS

FRP-RC bridge deck slabs, hybrid FRP tendon, prestress, static behavior, utilization efficiency

1 | INTRODUCTION

Bridge decks reinforced with fiber reinforced polymer (FRP) tendons have been widely investigated and applied over the past 20 years.^{1–9} Moreover, the design and construction methods of FRP-RC bridge deck slabs are proposed in the existing literature.^{10,11} Because of the relatively low stiffness of FRP composites, especially GFRP, RC members reinforced with FRP based on the equivalent strength principle exhibit larger deflections and crack widths than the

conventional steel-reinforced members.^{1,12} Consequently, the design of bridge decks reinforced with FRP composites is controlled by serviceability limit state rather than ultimate limit state.⁹ In such circumstances, to fulfill the requirements of serviceability limits, the equivalent reinforcement stiffness should be maintained similar to that in RC bridge decks, according to CSA.¹³ Therefore, in its empirical design method, CSA recommends a minimum reinforcement ratio of transverse FRP bars with equivalent stiffness to the steel bars with a reinforcement ratio of 0.25%. However, the deck slabs designed according to CSA failed in punching shear with carrying capacities significantly higher than the red design load,⁴ which reflects a large material waste in the

Discussion on this paper must be submitted within two months of the print publication. The discussion will then be published in print, along with the authors' closure, if any, approximately nine months after the print publication.

design of FRP-RC bridge decks. One approach to overcome this design shortcoming is to introduce prestressing method into the design of the FRP-RC deck slabs.

Because of the composite action between the deck slab and the supporting girders, the stress transfer in the deck slab is similar to the well-known arching action/compressive membrane action in RC beams, which greatly enhances the load-carrying capacity of deck slabs.^{14,15} The transverse prestressing of bridge deck slabs can further increase the compressive membrane stresses and lead to a thinner deck with improved serviceability and capacity.¹⁶ RC deck slab models that were fully prestressed by FRP tendons were investigated by Braimah et al.,¹⁴ who concluded that bridge deck slabs without any steel reinforcement performed satisfactorily in both capacity and deformation. The aforementioned studies were conducted on scaled models due to cost and space limitations. It should be noted that in contrast to fully prestressed concrete, the advantages of partially prestressed concrete include increased ductility and energy absorption capability, improved cost-efficiency and a reduction of the camber generated by prestressing.¹⁷

The selection of different types of fibers of FRP in FRP-RC deck slabs is another option for the optimization of deck slab. For instance, CFRP bars and GFRP bars were the foremost choices in previous studies. CFRP exhibits a relatively high modulus but has a high cost, while GFRP exhibits much low costs but has a low modulus. Furthermore, due to its low-creep rupture limit ($0.3f_u$ according to ACI-440.1R¹⁸), GFRP is not suitable for prestressing tendons. To overcome these problems, hybrid FRP composites were developed by different researchers.^{19–24} The hybridization of different types of fibers could overcome their shortcomings, integrate their advantages, and consequently achieve a high performance-to-price ratio. In addition, through hybridization, the mechanical properties of the FRP composites can be designed for specific applications.^{22,25} Therefore, based on the existing deficiencies of bridge deck slab, this study aims to enhance the utilization efficiency of FRP reinforcement in FRP-RC deck slabs by using prestressing technology and hybrid FRP tendons.

2 | EXPERIMENTAL PROGRAM

2.1 | Material properties

Three types of reinforcements were used in this study: steel, glass FRP (GFRP), and basalt/carbon (abbreviated as B/C) hybrid FRP bars. All of the FRP bars had a fiber content of 60% by volume impregnated with a vinyl ester resin and were produced via a pultrusion process. The hybrid FRP bars had a B/C ratio of 1:1, with carbon located at the core of the bar with a diameter of 7 mm for 10 mm B/C hybrid bars, and with a diameter of 8.5 mm for 12 mm B/C hybrid bars. The transversal section and the external surface of the

hybrid B/C bar and GFRP bar are shown in Figure 1. The prestressed hybrid reinforcements were identical with the nonprestressed ones in the prestressed slabs, except for their diameters. The mechanical properties of the steel, GFRP, and B/C hybrid bars are listed in Table 1. The slabs were cast using C40 ready-mixed concrete with a target 28-day concrete strength of 30 MPa. During the casting process, it was observed that the consistency of the concrete differed from one slab to another one. Thus, three cylinders (150 mm diameter and 300 mm height) were cast for each slab to determine the concrete strength. The average axial compressive strengths of concrete for different slabs, obtained on the day of slab testing, are listed in Table 2.

2.2 | Test specimens

A total of seven full-scale RC deck slabs were prepared. The slabs were square in plane, with a 2,400 mm side length and a 200 mm thickness. The 2,400 mm length of the specimens was determined considering the space of the reaction frame (see Section 2.4). The value of 2,400 mm did not exceed the maximum limit of the span (4,000 mm) recommended by CSA.¹³ The 200 mm thickness was determined according to the empirical span/thickness ratio (ranging from 12 to 15) of bridge deck slab. Five slabs were partially prestressed with B/C hybrid FRP tendons, and the other two slabs served as control slabs without prestressing. The reinforcement details of each specimen are listed in Table 2. The reinforcements of the two nonprestressed control slabs were designed according to the empirical design method of CSA.¹³ The prestressed FRP-RC deck slabs were designed according to three parameters: the FRP-reduction factor (RF = reduction in the FRP transverse reinforcement area with respect to the FRP-RC control slab), the prestressing level (P % = the ratio of prestress force to tensile capacity, in percentage), and the partial prestressing index (PPI = ratio of the prestressed FRP reinforcement to the total FRP reinforcement in the transverse direction of the slab). Three different RF values, namely, 0.45, 0.37, and 0.29, were considered in this study. The FRP tendons were tensioned to 35 or 50% of their ultimate strength, considering the high-creep rupture limit of BFRPs (52% of its ultimate strength), which allows them be used as highly efficient prestressing materials.^{26,27} Two PPIs of 0.5 and 0.6 were adopted in this study. In a previous study, El-Gamal et al.⁴ found that the upper reinforcements had a negligible effect on the static behavior of bridge deck slabs. Therefore, all of the tested slabs were designed without upper reinforcement. A minimum bottom clear cover of 25 mm, as specified by CSA,¹³ was determined for all specimens.

The typical dimensions, axial stiffness, and details of reinforcement of steel and FRP-RC deck slabs are shown in Figure 1 and Table 2. The prestressed specimens were identified according to their FRP-reduction factor, prestress level and PPI value.

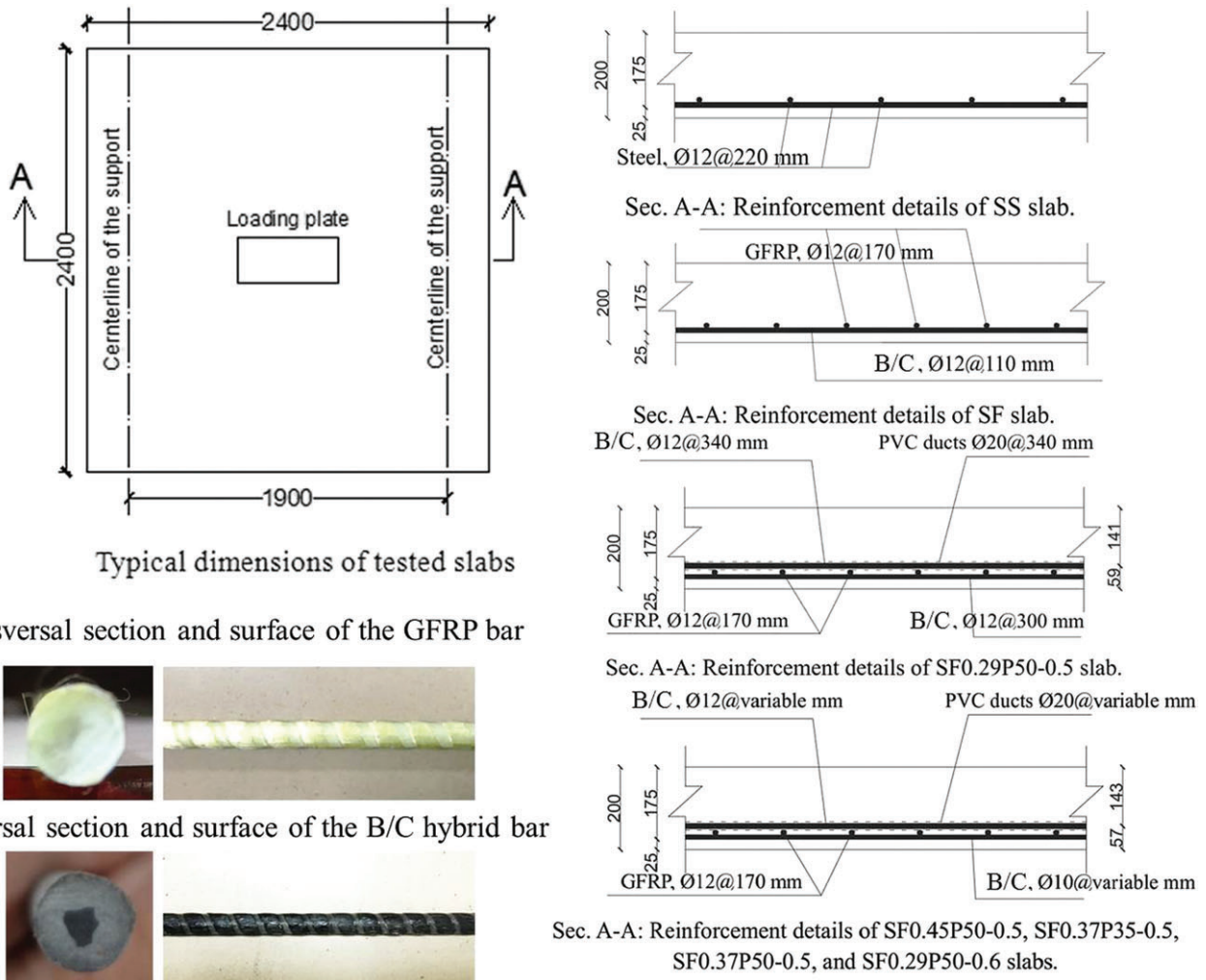


FIGURE 1 Dimensions of the specimens and details of the reinforcements

2.3 | Anchoring and prestressing system

Bonded prestressing was adopted in this study to reduce the losses of the prestressing force with respect to time. Deformed PVC tubes with 20 mm inner diameters were used as ducts, as shown in Figure 2. Two vertical PVC tubes with 20 mm inner diameters were connected to the horizontal PVC ducts and used for grout filling. The prestressing anchorage system was composed of steel sleeves filled with epoxy resin, with 250 mm lengths, 35 mm outer diameters, and 10 mm wall thicknesses. One end of the FRP tendons was first anchored with one steel sleeve and then the FRP tendon was inserted into the PVC duct. Then the other end of the FRP tendon was bonded to another steel sleeve.

TABLE 1 Mechanical properties of the reinforcing bars

Bar type (ID)	Diameter (mm)	Tensile strength (MPa)	Modulus of elasticity (GPa)	Ultimate strain (%)
Steel ^a	12	400 (yield)	200	0.2 (yield)
B/C	10	1,375	94	1.45
B/C	12	1,370	94	1.45
Glass	12	1,170	48	2.40

^a The properties of steel bars are provided by the manufacturer.

Figure 3 shows the details of both the anchor end and tensioning end of the prestressing tendons. At the anchor end, the anchorage was contacted with the bearing steel plate ($200 \times 200 \times 10 \text{ mm}^3$) by a steel nut. At the tensioning end, a 300 kN hydraulic jack acting on a stiff anchorage chair and bearing against a steel nut was used to tension the hybrid FRP tendon. Once the desired prestress jacking force was reached, another steel nut was used to anchor the tendon. The tendons in the PVC tubes were then grouted with cement rich grout. The slabs were tested 2 months after they were grouted to consider the losses caused by the initial relaxation of tendon and the creep of concrete.

2.4 | Test setup

All bridge deck slabs were tested under a concentrated load using a two-actuator loading machine. The two actuators were connected to a stiff steel beam that transferred the load to the loading steel plate. The concentrated load was applied through a 10-mm-thick neoprene pad placed beneath a 60-mm-thick steel plate. Both the neoprene pad and the steel plate were rectangular ($600 \text{ mm} \times 250 \text{ mm}$) in shape, simulating the contact area of the CL-625 Truck wheel load of

TABLE 2 Concrete strength and details of the reinforcements

Specimen number	Concrete strength, f_c (MPa)	Longitudinal reinforcement	Transverse reinforcement		FRP-reduction factor (RF)	Partial prestressing index (PPI)	Prestress level (P %)
			Nonprestressed	Prestressed			
SS ^a	26.8	Steel, Ø12@220	Steel, Ø12@220	N.A.	N.A.	N.A.	N.A.
SF ^b	27.1	GFRP, Ø12@170	B/C, Ø12@110	N.A.	N.A.	N.A.	N.A.
SF0.45P50-0.5	27.3	GFRP, Ø12@170	B/C, Ø10@300	B/C, Ø12@400	0.45	0.50	50
SF0.37P35-0.5 ^c	26.9	GFRP, Ø12@170	B/C, Ø10@265	B/C, Ø12@340	0.37	0.50	35
SF0.37P50-0.5	27.3	GFRP, Ø12@170	B/C, Ø10@265	B/C, Ø12@340	0.37	0.50	50
SF0.29P50-0.5	21.1	GFRP, Ø12@170	B/C, Ø12@300	B/C, Ø12@340	0.29	0.50	50
SF0.29P50-0.6	26.7	GFRP, Ø12@170	B/C, Ø10@265	B/C, Ø12@265	0.29	0.60	50

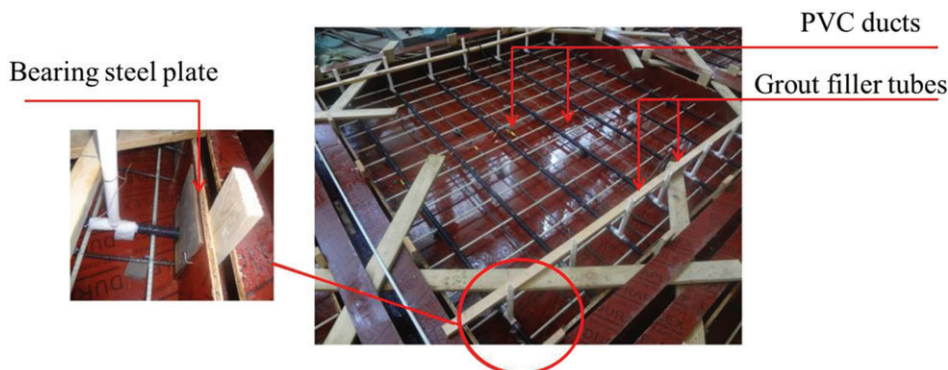
^a SS denotes steel-RC bridge deck.^b SF denotes nonprestressed FRP-RC bridge deck.^c SF0.37P35-0.5 denotes prestressed FRP-RC bridge deck with reduction factor equal to 0.37, prestress level of 35% and PPI value of 0.5.

FIGURE 2 The prestressing ducts and the grout filling system

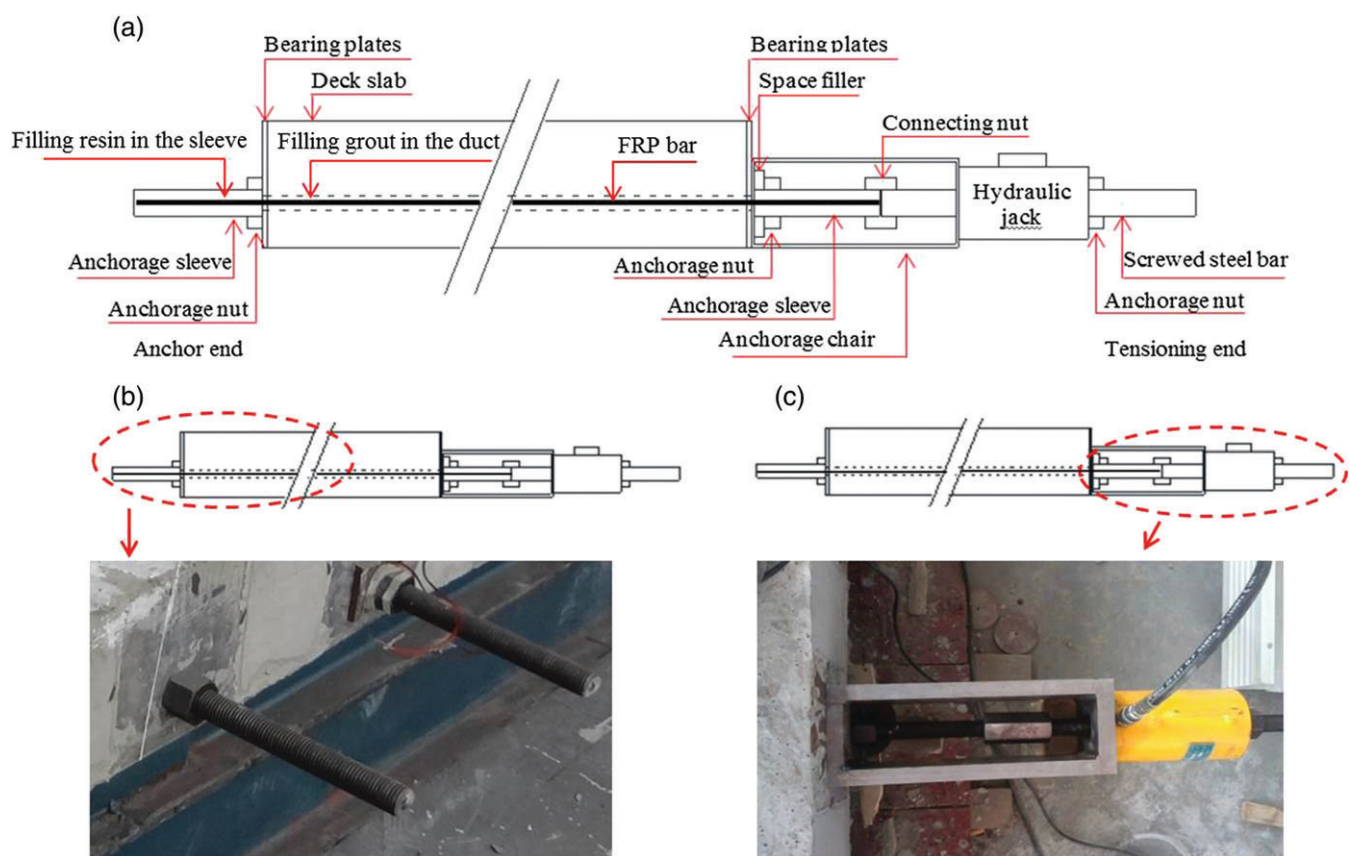


FIGURE 3 Prestressing setup (a) prestressing method (b) the anchor end (c) the tensioning end

87.5 kN, as specified by CSA.¹³ CL-625 Truck is one of the most commonly used vehicle type in CSA code. The slabs were simply supported on two steel beams spaced at 1900 mm on center. The steel beams transferred the load to the laboratory rigid floor. Figure 4 shows a photo and a schematic drawing of the test setup.

2.5 | Loading procedure and measurements

The slabs were first precracked through loading up to 200 kN and were then unloaded to 5 kN. The slabs were loaded up to failure during the second loading procedure. The load was applied with a constant loading rate of 5 kN/min during both of the loading stages.

The longitudinal and transverse deflection profiles of the slabs were measured by a series of linear variable displacement transducers located at different positions under the tested slabs. At the end of the first loading procedure, the initial crack widths were measured manually using a 50× handheld microscope. Then, PI-gauges were installed at three largest cracks to measure the crack width electronically with an increasing load during the second loading procedure. The largest value of the measured crack widths was selected and considered in the analysis. Electrical strain gauges were installed on the reinforcement bars to measure the reinforcement strains. Moreover, two electrical strain gauges were glued to the upper surface of the slab near the loading plate to measure the concrete strains. Three digital cameras were located under the slab to monitor the initiation of the first cracks. The values of deflections, strains, and crack widths were collected by TDS-530 data logger.

3 | TESTS RESULTS AND DISCUSSION

Table 3 summarizes the test results. According to CSA,¹³ the maximum wheel load of the design truck (CL-625 Truck) is 87.5 kN. Thus, the design service load P_{ser} of the deck slabs was determined by $1.4 \times 0.9 \times 87.5 = 110.25$ kN, where 1.4 is the impact coefficient and 0.9 is the live

load combination factor. Further, the design factored load was taken as $1.4 \times 1.7 \times 87.5 = 208.25$ kN, where 1.7 is the live load factor. Note that the results in this study are only available for simply supported bridge deck slab. For the slab crosses the girders continuously, appropriated reinforcements must be arranged at the upper side to resist the tensile stress at supports.

3.1 | Mode of failure and cracking behavior

Although the longitudinal flexural cracks were dominant up to the failure load, the tested slabs failed in punching or flexural/punching modes (Figure 5). The control slab reinforced with steel bars (SS) failed in flexural/punching mode after yielding of steel bars and exhibited a larger number of cracks with smaller spacing (Figure 6). The nonprestressed FRP-RC control slab, however, failed in punching failure mode which is consistent with the observation by other researchers.^{3,4,14} Because the two control deck slabs had almost identical reinforcement stiffness at the transverse direction, the difference in the failure mode reflects the superior load distribution realized by steel bars, which allows the whole slab to resist the applied load. Furthermore, the prestressed and nonprestressed FRP-RC slabs exhibited no obvious differences in crack patterns (Figure 6). The prestressed FRP-RC slabs also failed in punching failure mode, except for the SF0.29P50-0.5 slab, which failed in flexural/punching mode. The failure mode of SF0.29P50-0.5 may be related to the relatively low-concrete strength used in the slab. These results indicate that the prestressing level, partial prestressing index, and FRP-reduction factor all have negligible effects on the failure mode of the prestressed FRP-RC bridge deck slabs.

Figure 7 indicates that the nonprestressed transverse reinforcements exhibited a more severe fragmentation compared to the damage of the prestressed tendons. This behavior was related to the debonding of the prestressed tendons, which led to a stress distribution along the entire length of the tendons. The debonding was caused by the leakiness of the

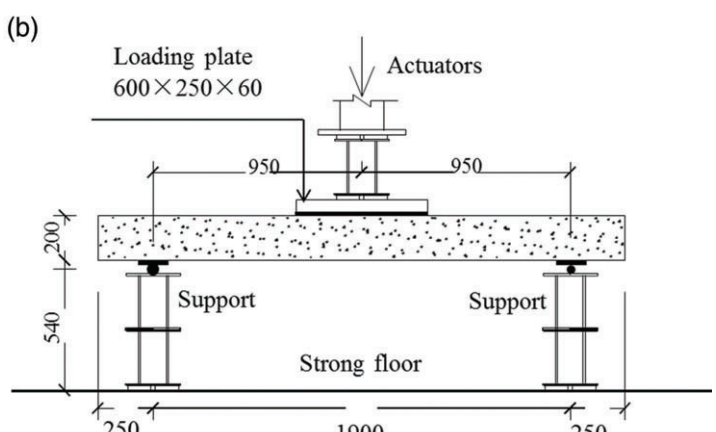


FIGURE 4 Test setup (a) photograph (b) schematic drawing

TABLE 3 Summary of the test results

Specimen number	Service					Ultimate				
	Cracking load (kN)	Ultimate load (kN)	Deflection (mm)	Crack width (mm)	Strains ($\mu\epsilon$)		Deflection (mm)	Crack width (mm)	Strains ($\mu\epsilon$)	
					FRP/steel	Concrete			FRP/steel	Concrete
SS	131	423	1.44	0.18	263	-125	37.8	3.07	>12,000	-2,366
SF	85	627	2.28	0.41	686	-192	30.7	1.10	6,610	-2,146
SF0.45P50-0.5	147	571	1.32	0.29	66	-189	34.6	1.80	8,438	-2,404
SF0.37P35-0.5	98	536	1.86	0.42	75	-182	39.5	3.56	10,762	-2,327
SF0.37P50-0.5	184	662	1.20	0.25	7	-130	33.9	1.86	6,911	-1,980
SF0.29P50-0.5	163	601	1.26	0.12	5	-99	30.7	1.84	6,177	-2,643
SF0.29P50-0.6	192	718	1.28	0.12	7	-28	25.2	2.08	7,362	-2,233

filled grout, and it occurred on the specimens numbered as SF0.45P50-0.5 and SF0.37P35-0.5. The rupture of the prestressed reinforcements would be as violent as the nonprestressed ones if debonding did not occur. The debonding should be avoided in practical engineering since it may have an impact on the capacity of structure. In addition, the fragmentation of the reinforcement of (SF) slab was much less than that of the prestressed slabs. That behavior was attributed to the higher reinforcement ratio in the control slab (SF).

3.2 | Cracking and ultimate loads

Table 3 shows that only two specimens, SF and SF0.37P35-0.5, had cracking loads lower than the design service load ($P_{ser} = 110.25$ kN). The cracking load of the other specimens ranged from 131 to 192 kN. The cracking load of SF slab was 35% lower than the cracking load of SS slab, which was caused by the difference in reinforcement distribution among the slabs and by the bonding characteristics of the FRP and steel reinforcements. The cracking loads

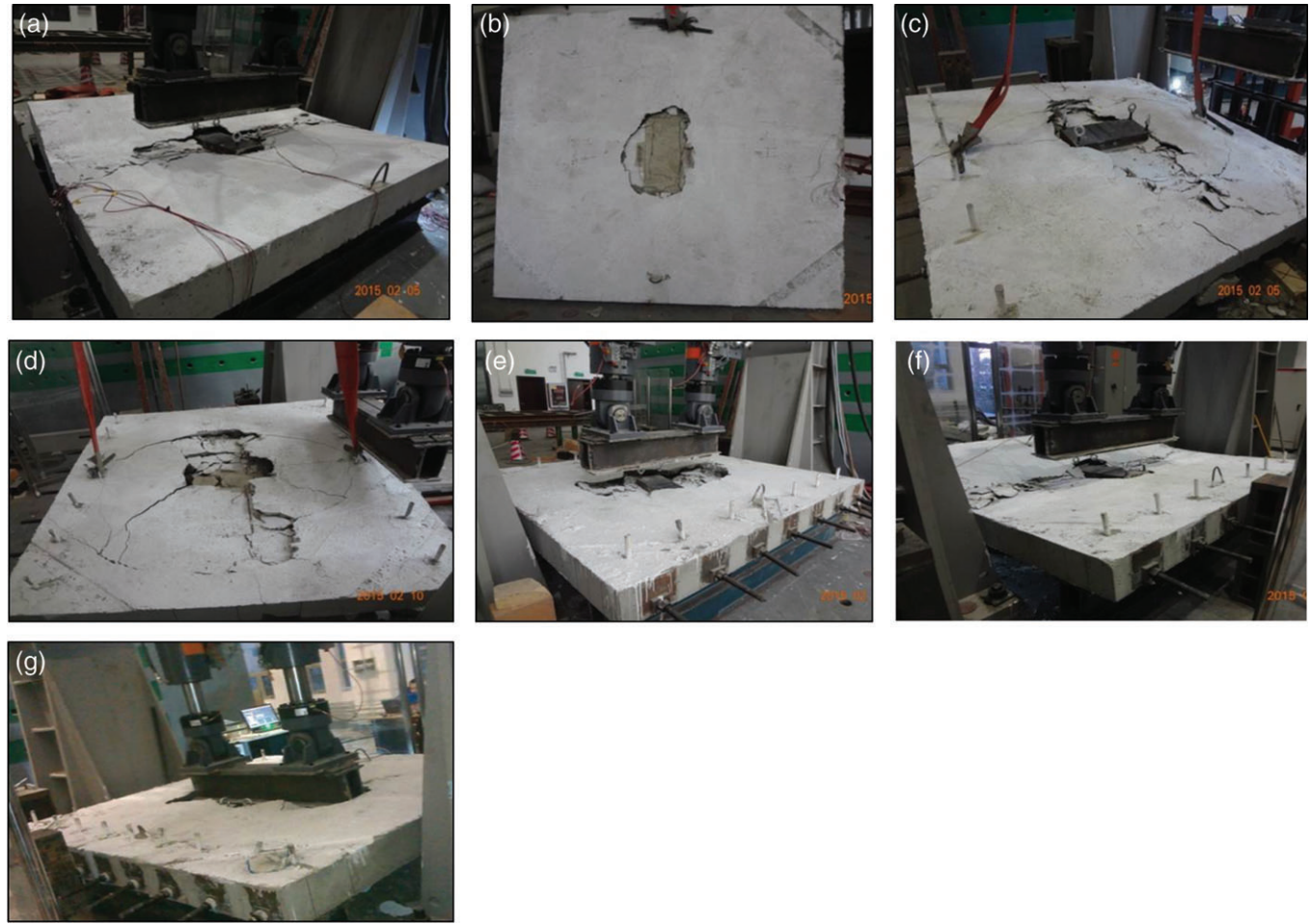
**FIGURE 5** Failure modes of (a) SS (b) SF (c) SF0.45P50-0.5 (d) SF0.37P35-0.5 (e) SF0.37P50-0.5 (f) SF0.29P50-0.5 (g) SF0.29P50-0.6



FIGURE 6 Crack pattern of (a) SS (b) SF and (c) SF0.37P35-0.5 slab

of the prestressed FRP-RC slabs were 15–126% higher than that of the SF control slab. Referring to the results of SF0.45P50-0.5 and SF0.37P50-0.5 slabs, it can be noted that increasing the reinforcement by 15% increased the cracking load by 25%. This effect was related to the increase of the concrete compressive stress of SF0.37P50-0.5, which depends on the reinforcement ratio. The relatively low-cracking load of slab SF0.29P50-0.5 was related to its low-concrete strength. Moreover, the results indicated that increasing the prestressing level by 15% increased the cracking load by 88%. Thus, the effect of prestressing level on cracking load is more significant than is the effect of FRP-reduction factor.

Table 3 shows that the failure load of the nonprestressed FRP-RC deck slab is three times higher than the design factored load of 208.25 kN recommended by the CSA¹³ due to the high strength of FRP reinforcement. This performance is consistent with that the tests by El-Gamal et al.^{3,4} The failure loads of the prestressed FRP-RC deck slab are 2.6–3.4 times higher than the design factored load. Referring to SF0.45P50-0.5 and SF0.37P50-0.5, increasing the reinforcement only by 15% increased the ultimate capacity by approximately 16%. In contrast, comparing SF0.37P35-0.5 with SF0.37P50-0.5 indicates that increasing the prestressing level by 43% only increased the ultimate capacity by 24%. Thus, reinforcement amount has a significant effect on the

ultimate loads, whereas the effect of the prestressing level is slight. CSA provides Equation (1) to calculate the punching capacity.

$$V_c = (\varphi_c f_{cr} + 0.25 f_{pc}) b_0 d + V_p, \quad (1)$$

where, φ_c is the material resistance factor taken as 0.75; f_{cr} is the cracking strength of concrete; f_{pc} is one-half the transverse concrete compressive stress; b_0 is the perimeter of critical section at a distance of $d/2$ from the loading plate; d is the distance from the extreme compression fiber to the centroid of the tension reinforcement; V_p is the vertical component of all effective prestress forces crossing the critical section which equals zero in this study. The ratios of the predicted punching capacity to the corresponding experimental data range from 0.95 to 1.19, which indicates a satisfactory accuracy of the calculation formula.

3.3 | Crack width

Figure 8 presents load-maximum crack width relationships for all test slabs. The values of crack widths at service and ultimate loads are presented in Table 3, in which the values were collected during the second loading procedure (after cracking). As shown in Figure 9, the crack widths at service load of the tested slabs ranged from 0.12 to 0.42 mm, less than the allowable code limits in CSA¹³ (0.5 mm). This result

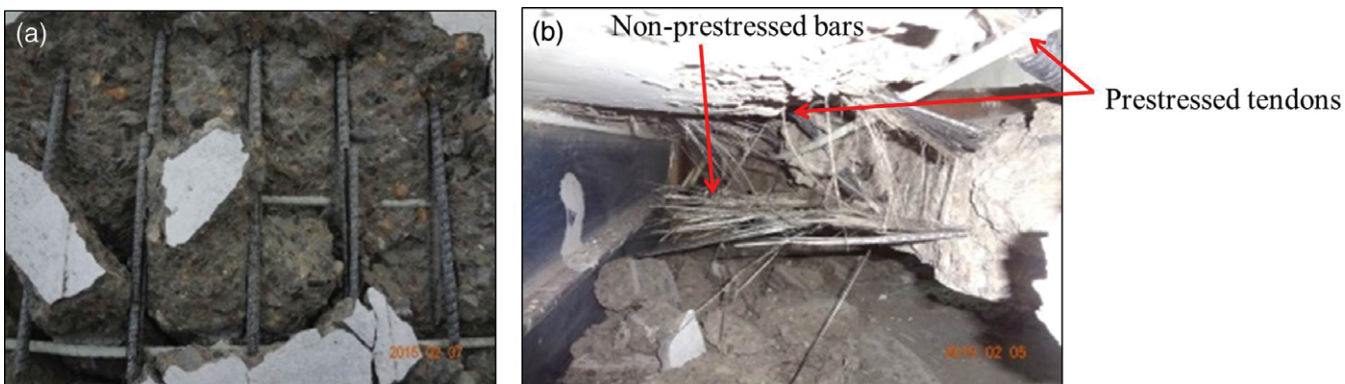


FIGURE 7 Damage of the reinforcements in (a) SF and (b) SF0.45P50-0.5

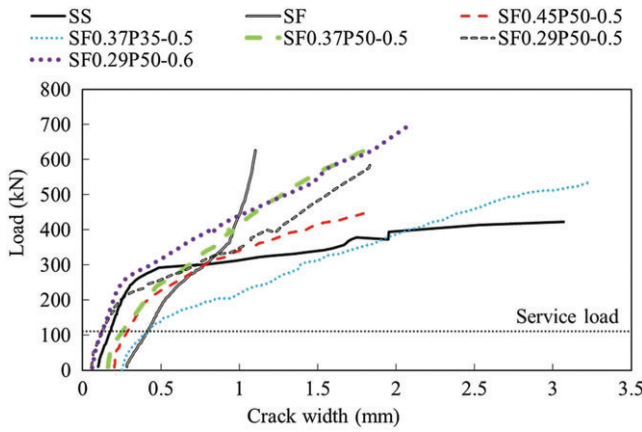


FIGURE 8 Load-maximum crack width curves

suggests that through a proper design method, the amount of FRP reinforcement can be reduced significantly and the crack width allowable limits can be guaranteed as well. SF0.37P35-0.5 slab exhibited the largest crack width at service load, whereas SF0.29P50-0.6 slab exhibited the smallest one. Although the two control slabs had the same reinforcement stiffness, the crack width at service load level of the SF slab was 2.28 times the crack width of the SS slab. This difference was caused by the dissimilar bonding characteristics of the two materials and the different reinforcement spacing between the two slabs. However, the SS slab exhibited larger cracks after yielding of the reinforcement. The crack width of SS slab at failure was 2.79 times the crack width of the SF slab. The crack widths at service and design load levels of the prestressed FRP-RC slabs, with PPI of 50%, were smaller than that of the control SF slab. However, at failure load, the SF slab presented a smaller crack width. It was found that the FRP-reduction factor significantly influenced the widths of cracks. The comparison between SF0.45P50-0.5 and SF0.29P50-0.5 shows that decreasing the FRP-reduction factor by 36% decreased the crack width at the service level by 59%. Again, this effect was related to the increase in the concrete compressive stress, which depends on the reinforcement ratio. Moreover, it was found that increasing the prestressing

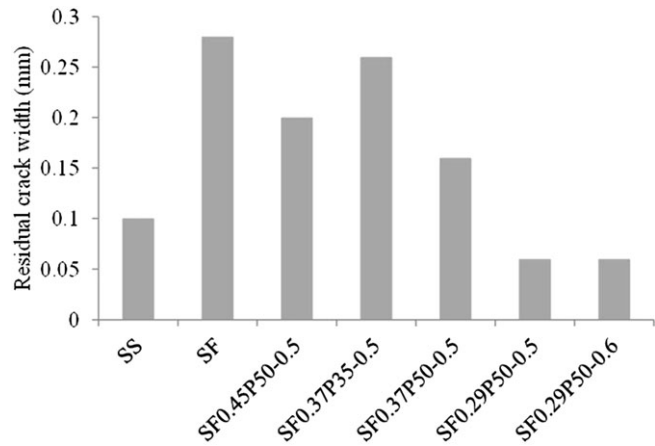


FIGURE 10 Residual crack widths

level from 35 to 50% decreased the crack width at the service load level by 40%. Thus, the FRP-reduction factor and pre-stressing level have significant effects on crack width. Furthermore, the results show that increasing the partial prestressing index by 10% has a negligible effect on the crack width at the service load level.

The initial value of the measured crack width at the finish of unloading in the first loading procedure, defined herein as the residual crack width (Figure 10), was taken as a primary index for the long-term behavior of the tested slabs. The results showed that the residual crack widths of all slabs prestressed with hybrid FRP tendons were smaller than that of the SF control slab, which indicates that the long-term performance of the prestressed FRP-RC deck slabs could be guaranteed. The residual crack width of SF0.45P50-0.5 slab was 29% smaller than that of the SF slab. Decreasing the FRP-reduction factor or increasing the prestressing level decreases the values of the residual crack width.

3.4 | Deflection

The load-maximum deflection curves of all test slabs are presented in Figure 11. The unloading stages were omitted for simplicity. A bilinear load-deflection behavior of FRP-

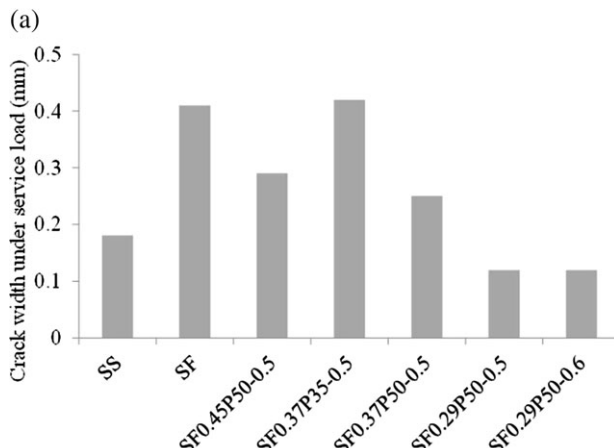
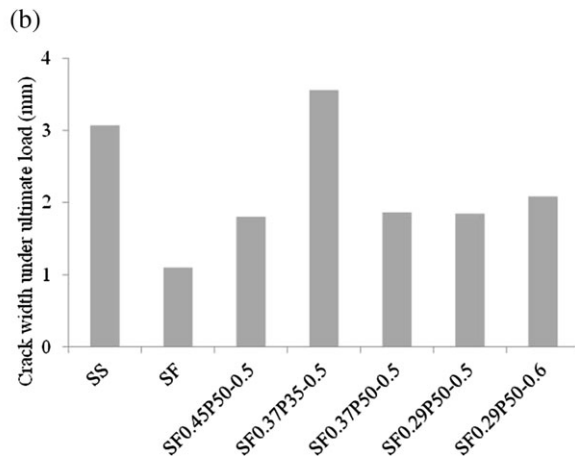


FIGURE 9 Crack widths at (a) service load and (b) ultimate load



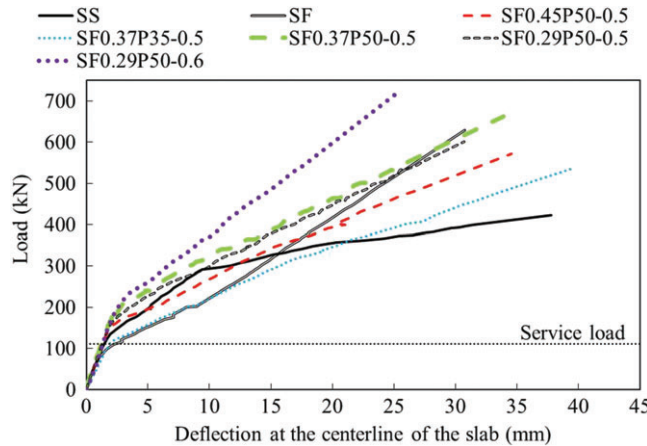


FIGURE 11 Load-maximum deflection curves

reinforced/prestressed concrete deck slabs is indicated by Figure 11. The first part up to the cracking load represents the behavior of the un-cracked slab with the gross inertia of the concrete cross section, and the second part represents the cracked slab with reduced inertia. The load-deflection curve of the steel-RC slab, however, was linear up to cracking load (131 kN), and it then displayed nonlinear behavior up to failure due to the cracking of concrete and the yielding of steel reinforcement. The load-maximum deflection relationships of the tested slabs were similar up to the service load level, beyond which the relationships differed significantly. For deck slabs that were prestressed with hybrid FRP tendons, SF0.29P50-0.6 slab had the highest postcracking stiffness, whereas SF0.37P35-0.5 slab exhibited the lowest. The results show that the postcracking stiffness increased significantly by increasing the reinforcement area or increasing the prestress level. The low-postcracking stiffness of SF0.29P50-0.5 slab compared to SF0.37P50-0.5 was attributed to the low-concrete strength of the former.

Figure 12 shows the deflections at the service and ultimate loads. The deflections at the service load level ($P_{ser} = 110.25$ kN) for the tested deck slabs ranged from

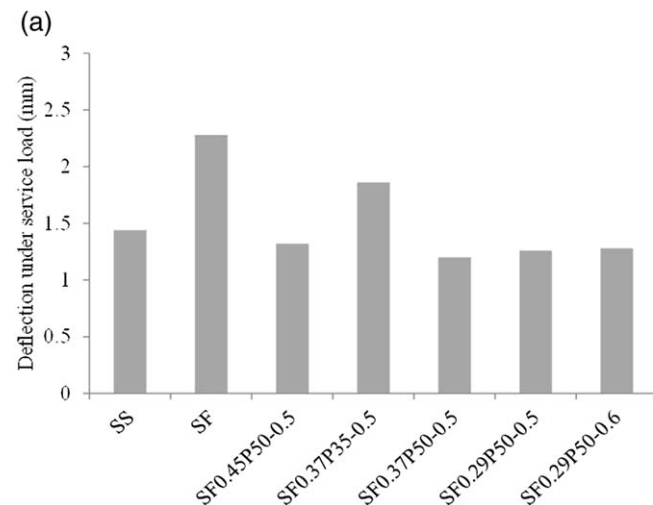


FIGURE 12 Deflections at (a) service load and (b) ultimate load

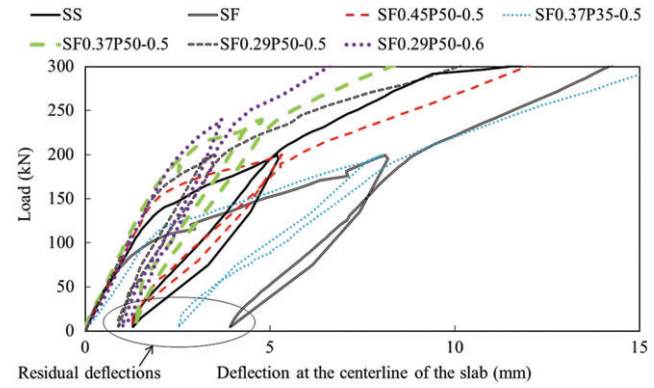
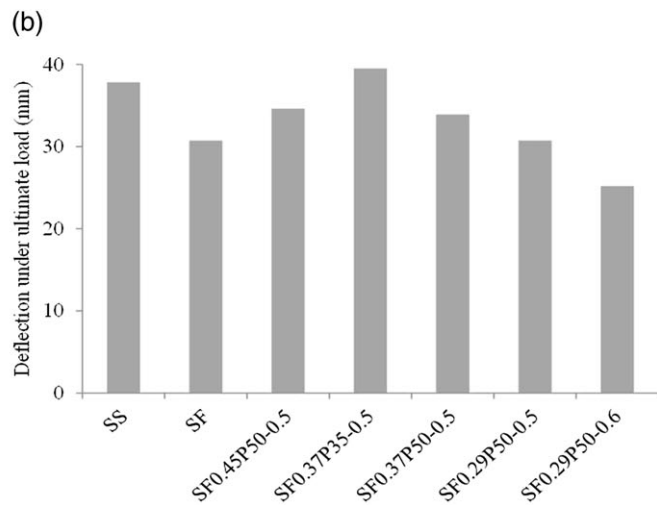


FIGURE 13 Load-maximum deflection curves including the unloading stages

1.20 to 2.28 mm, which were below the allowable limits (1/400 of the span).¹³ The control slab (SF) exhibited the largest deflection at the service load level, but it should be noted that due to continuity of the slab over the girders in the actual bridge deck, the deflections at the same load level are expected to be less than what was measured in the laboratory.² The FRP-reduction factor and the partial prestressing index have no effect on the deflection at the service load level. In fact, these slabs exhibited cracking loads higher than the service load level; therefore, the deflections of these slabs were controlled by the gross inertia of the concrete cross section. However, for SF0.37P35-0.5 slab, the cracking load was lower than the service load. Therefore, its deflection at the service level was larger than those of the other prestressed FRP-RC deck slabs.

The maximum deflection of the slabs at the end of the unloading stage is defined herein as residual deflection. Figures 13 and 14 show the residual deflections of the specimens. It can be noted that the steel-RC deck slab presented a smaller residual deflection than that of FRP-RC deck slab. In addition, all of the prestressed FRP-RC deck slabs had smaller residual deflections than that of SF



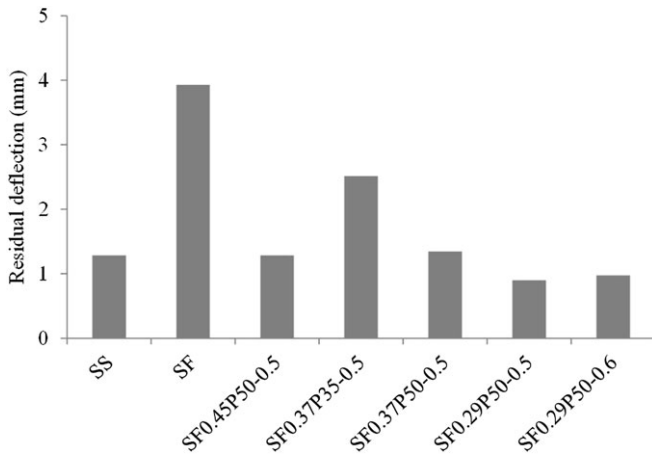


FIGURE 14 Residual deflections

control slab. Part of the prestressed FRP-RC deck slabs even exhibit less residual deflections than that of SS slab. Increasing the prestressing level significantly reduced the residual deflection, whereas increasing the FRP reinforcement or partial prestressing index had a slight effect on the residual deflection.

The deflection profiles along half of the transverse and longitudinal directions for the two control slabs and for SF0.45P50-0.5 slab are presented in Figure 15. In general, it can be stated that the initially flat slab deformed into a shallow cone outside the loaded area region. Along half of the longitudinal direction, the slab deflection can be well described as a result of rigid body rotation. Additionally, the deflection profile along the half longitudinal direction of steel-RC deck slab had a flat slope, whereas the FRP-RC control deck slab had a sharp slope. This behavior could be explained by the yielding of the steel reinforcement that allows stress distribution within the longitudinal direction of the slab. The slope of SF0.45P50-0.5 slab lay between the above two control slabs. Therefore, the prestressed FRP-RC slab not only presents a smaller crack width and maximum deflection but also has a more uniform stress distribution than does the nonprestressed FRP-RC control slab.

3.5 | Reinforcement and concrete strains

Table 3 presents the maximum strains in nonprestressed reinforcement and concrete at the service and ultimate load of the tested slabs. At the service level, the maximum

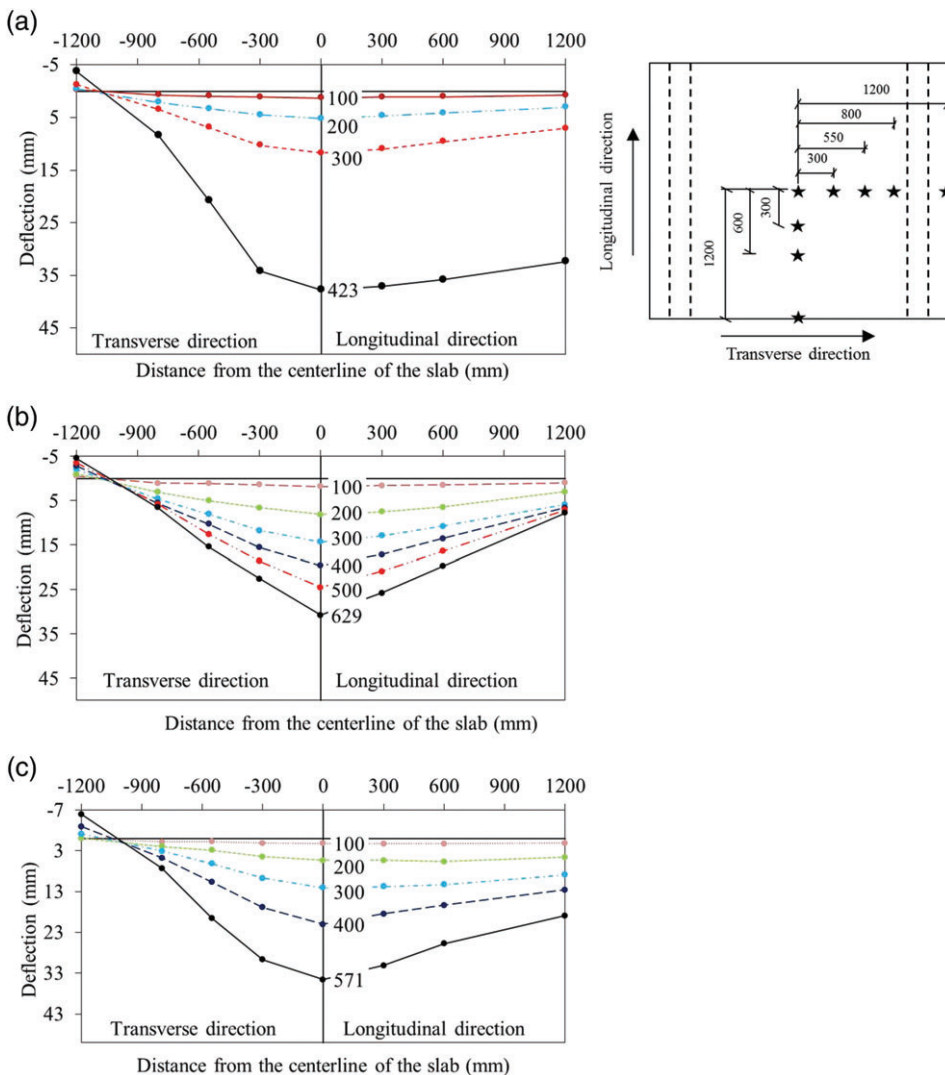


FIGURE 15 Deflection profiles along half of the transverse and longitudinal directions (a) SS (b) SF (c) SF0.45P50-0.5

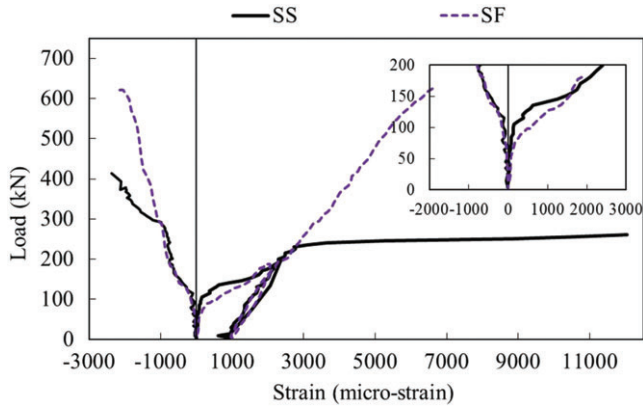


FIGURE 16 Reinforcement and concrete strains of the control slabs

measured strains of the steel and FRP reinforcement of the control slabs were 13% of the steel yield strain and 5% of the FRP ultimate strain, respectively. At failure level, the maximum measured strain of the steel reinforcement of SS slab was larger than its yielding strain; however, the maximum strain of the FRP reinforcement of the FRP-RC control deck slab was only 46% of its ultimate strain. This indicates that the bottom transverse reinforcement ratio used for the FRP-RC control deck slab according to the CSA¹³ is excessively conservative and can be reduced by an optimum design of such deck slabs. In addition, the strains of the nonprestressed FRP bars of the prestressed FRP-RC deck slabs were negligible at the service load level, whereas the strains ranged from 43 to 74% of their ultimate strain at the failure load level. Those results demonstrate that the fragmentation of the nonprestressed bars developed due to the shear stresses associated with the punching failure mode rather than due to the tensile stresses. Moreover, the strains of the nonprestressed bars decreased by increasing the prestressing level or decreasing the FRP-reduction factor. Furthermore, the concrete strains of the tested slabs at service level were less than 6.4% of its ultimate strain, but at failure level, the strain ranged from 66 to 88% of its ultimate value. These results also prove the punching mode failure of the tested slabs.

Figure 16 presents the maximum reinforcement and concrete strains of the two control slabs, SS and SF. The

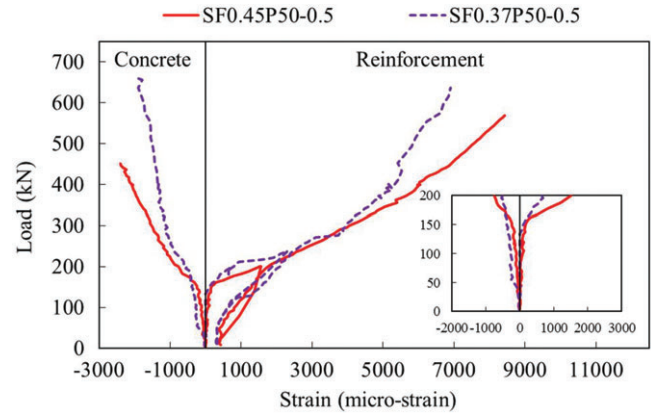


FIGURE 18 Effect of FRP-reduction factor on the strains of reinforcement and concrete

reinforcement strains of the two slabs are almost identical up to steel yielding. This behavior, in addition to the lower modulus of the FRP reinforcement compared to steel reinforcement, explains the larger deflection and crack width of the FRP-RC control deck slab compared to the steel-RC deck slab prior to the yielding of steel reinforcement. Beyond the yielding of steel, however, the FRP strains increased linearly up to failure. The concrete strain development of the two control slabs was similar to that of the reinforcement strains.

Figure 17 presents the effect of prestressing level on the strains of the nonprestressed reinforcement and concrete. This figure shows that increasing the prestressing level decreased not only the strains of the nonprestressed bars after the cracking of the concrete but also the residual strains upon load removal. In addition, Figure 18 demonstrates that decreasing the FRP-reduction factor decreased the strains of the nonprestressed bars after the concrete cracking. However, the FRP-reduction factor had a slight effect on the residual strains of the nonprestressed bars.

4 | CONCLUSIONS

The study presented an experimental investigation on the static behavior of RC deck slabs that were partially prestressed with hybrid FRP tendons. The effects of three main variables, namely, the FRP-reduction factor, prestress level, and partial prestressing index were studied. The results were presented in terms of crack patterns and failure modes, cracking and ultimate loads, deflections, crack widths, and strains of the reinforcement and concrete. Based on the aforementioned studies, the following major conclusions can be drawn.

1. By adoption of prestressing hybrid FRP tendons, not only the amount of FRP reinforcements in RC deck slab can be significantly decreased, but also the static behaviors of FRP-RC deck slab were significantly improved.

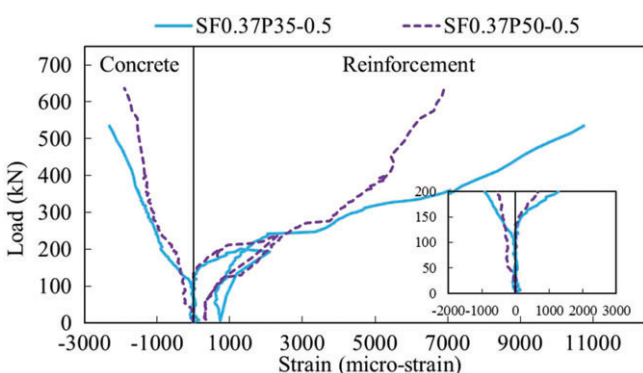


FIGURE 17 Effect of prestressing level on the strains of reinforcement and concrete

- Furthermore, the superior long-term behavior can be expected, as reflected by the small residual crack widths and deflections of prestressed FRP-RC deck slabs.
2. Flexural and punching shear was the failure mode of the nonprestressed steel-RC deck slabs, whereas the failure of both nonprestressed and partially prestressed FRP-RC deck slabs was characterized by the punching failure mode. Prestressing level, partial prestressing index, and FRP-reduction factor have no effect on the failure mode of the prestressed FRP-RC bridge deck slabs.
 3. Higher prestressing level increases cracking loads significantly, but has minimal effect on the ultimate load. The increase of prestressing level contributes to smaller deflection and crack width at both service load and ultimate load. Moreover, higher prestressing levels restrict the strains in nonprestressing reinforcements noticeably but have negligible effects on the strains in concrete. In contrast, increasing the PPI by 10% has a negligible effect on the static behaviors of FRP-RC deck slabs.
 4. For prestressed FRP-RC deck slabs, a smaller FRP-reduction factor, which means more prestressing FRP reinforcement, causes a significantly smaller crack width at service load, smaller strain in nonprestressing reinforcements and concrete, larger ultimate and cracking loads. However, the effects of the FRP-reduction factor on deflection and crack width at ultimate load can be neglected.

ACKNOWLEDGMENTS

The authors gratefully acknowledge the financial support provided by the National Key Research and Development Program of China (2017YFC0703000), the Natural Science Foundation of Jiangsu Province (BK20150886), the National Natural Science Foundation of China (NSFC 51678139 and 51508277) and acknowledge Jiangsu GMV Co., Ltd. for providing FRP tendons.

ORCID

Xin Wang  <http://orcid.org/0000-0003-4504-8502>

REFERENCES

1. Michaluk CR, Rizkalla SH, Tadros G, et al. Flexural behavior of one-way concrete slabs reinforced by fiber reinforced plastic reinforcements. *ACI Struct J.* 1998;95(3):353–365.
2. El-Salakawy EF, Benmokrane B. Serviceability of concrete bridge deck slabs reinforced with FRP composite bars. *ACI Struct J.* 2004;101(5):727–736.
3. El-Gamal S, El-Salakawy E, Benmokrane B. Behavior of concrete bridge deck slabs reinforced with fiber-reinforced polymer bars under concentrated loads. *ACI Struct J.* 2005;102(5):727.
4. El-Gamal S, El-Salakawy E, Benmokrane B. Influence of reinforcement on the behavior of concrete bridge deck slabs reinforced with FRP bars. *J Compos Constr.* 2007;11(5):449–458.
5. Hassan T, Abdelrahman A, Tadros G, Rizkalla S. Fibre reinforced polymer reinforcing bars for bridge decks. *Can J Civ Eng.* 2000;27(5):839–849.
6. Matthys S, Taerwe L. Concrete slabs reinforced with FRP grids. II: Punching resistance. *J Compos Constr.* 2000;4(3):154–161.
7. Pirayeh GS, Head M, Hurlebaus S, et al. Comparative experimental performance of bridge deck slabs with AFRP and steel precast panels. *J Compos Constr.* 2013;17(6):04013014.
8. Rahman AH, Kingsley CY, Kobayashi K. Service and ultimate load behavior of bridge deck reinforced with carbon FRP grid. *J Compos Constr.* 2000;4(1):16–23.
9. Yost J, Schmeckpeper E. Strength and serviceability of FRP grid reinforced bridge decks. *J Bridg Eng.* 2001;6(6):605–612.
10. Benmokrane B, El-Salakawy E, El-Ragaby A, et al. Designing and testing of concrete bridge decks reinforced with glass FRP bars. *J Bridg Eng.* 2006;11(2):217–229.
11. Ahmed EA, Settecaso F, Benmokrane B. Construction and testing of GFRP steel hybrid-reinforced concrete bridge-deck slabs of Sainte-Catherine overpass bridges. *J Bridg Eng.* 2014;19(6):04014011.
12. Ombres L, Alkhraiji T, Nanni A. *Flexural analysis of one way concrete slabs reinforced with GFRP rebars*. PLAST: International meeting on composite materials, 2000;p. 243–250.
13. CSA-S6-2014. *Canadian highway bridge design code*. Rexdale, ON: Canadian Standards Association (CSA), 2014.
14. Braimah A, Green MF, Soudki KA. Polypropylene FRC bridge deck slabs transversely prestressed with CFRP tendons. *J Compos Constr.* 1998;2(4):149–157.
15. Moll EL. Investigation of transverse stressing in bridge decks [ME thesis]. Hamilton: McMaster University; 1984.
16. Savides P. Punching shear strength of transversely prestressed deck slabs of composite I-beam bridges [MS thesis]. Kingston: Queen's University at Kingston; 1989.
17. Chern JC, You CM, Bazant ZP. Deformation of progressively cracking partially prestressed concrete beams. *PCI J.* 1992;37(1):74–85.
18. ACI 440.4R-04. *Prestressing concrete structures with FRP tendons*. Farmington Hills, MI: American Concrete Institute, 2004.
19. Bunsell AR, Harris B. Hybrid carbon and glass fibre composites. *Composites*. 1974;5(4):157–164.
20. Harris HG, Somboonsong W, Ko FK. New ductile hybrid FRP reinforcing bar for concrete structures. *J Compos Constr.* 1998;2(1):28–37.
21. Manders PW, Bader MG. The strength of hybrid glass/carbon fibre composites. *J Mater Sci.* 1981;16(8):2233–2245.
22. Ali NM, Wang X, Wu Z. Integrated performance of FRP tendons with fiber hybridization. *J Compos Constr.* 2014;18(3):A4013007.
23. Tepfers R, Tamuis V, Apinis R, et al. Ductility of nonmetallic hybrid fiber composite reinforcement for concrete. *Mech Compos Mater.* 1996;32(2):113–121.
24. You YJ, Park YH, Kim HY, Park JS. Hybrid effect on tensile properties of FRP rods with various material compositions. *Compos Struct.* 2007;80:117–122.
25. Wang X, Wu Z, Wu G, Zhu H, Zen F. Enhancement of basalt FRP by hybridization for long-span cable-stayed bridge. *Compos Part B*. 2013;44:184–192.
26. Wang X, Shi J, Liu J, Yang L, Wu Z. Creep behavior of basalt fiber reinforced polymer tendons for prestressing application. *Mater Des.* 2014;59:558–564.
27. Wang X, Shi J, Wu G, Yang L, Wu Z. Effectiveness of basalt FRP tendons for strengthening of RC beams through the external prestressing technique. *Eng Struct.* 2015;101:34–44.

AUTHOR'S BIOGRAPHIES



Xin Wang, Professor
Key Laboratory of C & PC
Structures Ministry of Education,
Southeast University, Nanjing,
210096, China
xinwang@seu.edu.cn



Nageh M. Ali, Ph.D. Candidate
Key Laboratory of C & PC
Structures Ministry of Education,
Southeast University, Nanjing,
210096, China



Lining Ding, Lecturer
School of Civil Engineering,
Nanjing Forestry University,
Nanjing 210037, China



Jianzhe Shi, Ph.D. Candidate
Key Laboratory of C & PC
Structures Ministry of Education,
Southeast University, Nanjing,
210096, China



Zhishen Wu, Professor
Key Laboratory of C & PC
Structures Ministry of Education,
Southeast University, Nanjing,
210096, China
zswu@seu.edu.cn

How to cite this article: Wang X, Ali NM, Ding L, Shi J, Wu Z. Static behavior of RC deck slabs partially prestressed with hybrid fiber reinforced polymer tendons. *Structural Concrete*. 2018;1–13. <https://doi.org/10.1002/suco.201700240>